



Original Article

Remedy for ill-posedness and mass conservation error of 1D incompressible two-fluid model with artificial viscosities

Byoung Jae Kim ^{a,*}, Seung Wook Lee ^b, Kyung Doo Kim ^b^a Department of Mechanical Engineering, Chungnam National University, 99 Daehak-ro, Yuseong-gu, Daejeon, 34134, Republic of Korea^b Thermal-Hydraulics System Safety Research Division, Korea Atomic Energy Research Institute, 111, Daedeok-daero 989Beon-gil, Yuseong-gu, Daejeon, 34057, Republic of Korea

ARTICLE INFO

Article history:

Received 1 April 2022

Received in revised form

28 May 2022

Accepted 22 June 2022

Available online 4 July 2022

Keywords:

Two-fluid model

Ill-posedness

Artificial viscosity

Mass conservation

ABSTRACT

The two-fluid model is widely used to describe two-phase flows in complex systems such as nuclear reactors. Although the two-phase flow was successfully simulated, the standard two-fluid model suffers from an ill-posed nature. There are several remedies for the ill-posedness of the one-dimensional (1D) two-fluid model; among those, artificial viscosity is the focus of this study. Some previous works added artificial diffusion terms to both mass and momentum equations to render the two-fluid model well-posed and demonstrated that this method provided a numerically converging model. However, they did not consider mass conservation, which is crucial for analyzing a closed reactor system. In fact, the total mass is not conserved in the previous models. This study improves the artificial viscosity model such that the 1D incompressible two-fluid model is well-posed, and the total mass is conserved. The water faucet and Kelvin-Helmholtz instability flows were simulated to test the effect of the proposed artificial viscosity model. The results indicate that the proposed artificial viscosity model effectively remedies the ill-posedness of the two-fluid model while maintaining a negligible total mass error.

© 2022 Korean Nuclear Society, Published by Elsevier Korea LLC. This is an open access article under the CC BY license (<http://creativecommons.org/licenses/by/4.0/>).

1. Introduction

The two-fluid model has been widely used to describe two-phase flows in complex systems such as nuclear reactors. The two-fluid model consists of two sets of conservation equations for the mass, momentum, and energy of the gas and liquid phases. Although two-phase flow has been successfully simulated, it is well known that the standard two-fluid model suffers from an ill-posed nature. The two-fluid model may not simulate the flow physics when the relative velocity between the two phases exceeds a critical value [1,2].

Various numerical/physics-based regularization methods have been studied to remedy the ill-posedness of the one-dimensional (1D) two-fluid model. These methods include the virtual mass [3], surface tension [2], hydrostatic pressure [4], interfacial pressure [5,6], two-pressure [7], interfacial velocity [8], flow distribution [9], and artificial viscosity [10]. This study focuses on artificial viscosity.

Artificial viscosity terms are often added to momentum equations to enhance numerical stability [11] and render the six-

equation two-fluid model well-posed [10]. Holmås et al. [12] were the first to add artificial axial diffusion terms to both the mass and momentum equations for 1D incompressible flow. They indicated that the addition of artificial diffusion terms to both the mass and momentum equations provided a numerically converging model for an incompressible flow. However, the physical meaning of artificial diffusion in the mass equation was not provided. Fullmer et al. [13] related the artificial diffusion terms to effective viscosities. Fullmer et al. [14] extended the artificial diffusion concept to create a model that prescribed the cutoff length scale.

The addition of artificial diffusion terms to both the mass and momentum equations effectively renders the two-fluid model well-posed. However, the previous studies did not consider the conservation of mass, which is crucial in the analysis of a closed reactor system. The mass error caused by the artificial diffusion terms in the mass equations must be examined.

The main purpose of this study is to improve the artificial viscosity model such that the 1D incompressible two-fluid model is well-posed and the total mass is conserved. The remainder of this paper is organized as follows. In Section 2, the previous artificial viscosity model is described, and an improved artificial viscosity model is proposed to resolve the mass conservation problem of the

* Corresponding author.

E-mail address: bjkim@cnu.ac.kr (B.J. Kim).

previous model. In Section 3, the water faucet problem and the Kelvin-Helmholtz instability are simulated to examine the effect of the proposed model. Finally, the conclusions are presented in Section 4.

2. Theory

2.1. Previous artificial viscosity model

The simplified mass and momentum equations for incompressible, isothermal, and inviscid flow in a constant-area channel [13] [14] are

$$\frac{\partial \alpha_g}{\partial t} + \frac{\partial}{\partial x} (\alpha_g u_g) = \varepsilon_g \frac{\partial^2 \alpha_g}{\partial x^2} \quad (1)$$

$$\frac{\partial \alpha_l}{\partial t} + \frac{\partial}{\partial x} (\alpha_l u_l) = \varepsilon_l \frac{\partial^2 \alpha_l}{\partial x^2} \quad (2)$$

$$\alpha_g \rho_g \left(\frac{\partial u_g}{\partial t} + u_g \frac{\partial u_g}{\partial x} \right) = -\alpha_g \frac{\partial p}{\partial x} + \rho_g \nu_g \frac{\partial}{\partial x} \left(\alpha_g \frac{\partial u_g}{\partial x} \right) + \alpha_g \rho_g g_x \quad (3)$$

$$\alpha_l \rho_l \left(\frac{\partial u_l}{\partial t} + u_l \frac{\partial u_l}{\partial x} \right) = -\alpha_l \frac{\partial p}{\partial x} + \rho_l \nu_l \frac{\partial}{\partial x} \left(\alpha_l \frac{\partial u_l}{\partial x} \right) + \alpha_l \rho_l g_x \quad (4)$$

where α , u , ε , ρ , p , ν , and g are the phasic fraction, velocity, artificial viscosity related to phase change, density, pressure, artificial viscosity, and gravity, respectively. Subscripts g and l indicate the gas and liquid phases, respectively. The momentum equations are expressed in the non-conservative form, and various force terms, such as interfacial drag, wall drag, and virtual mass effect, are omitted.

Equations (1)–(4) can be provided in the matrix form:

$$\mathbf{A} \frac{\partial \Psi}{\partial t} + \mathbf{B} \frac{\partial \Psi}{\partial x} + \mathbf{C} \frac{\partial^2 \Psi}{\partial x^2} + \mathbf{D} = 0 \quad (5)$$

where $\Psi = (\alpha_g \ u_g \ u_l \ p)$ is the vector of the independent variables. The evolution of Ψ is considered by assuming a small perturbation in the form of a traveling wave as follows:

$$\Psi = \Psi_0 + \delta \widehat{\Psi} \exp[i(kx - \omega t)] \quad (6)$$

where Ψ_0 is the reference state, $\delta \widehat{\Psi}$ is the vector of the perturbation amplitudes, k is the wavenumber, and ω is the growth rate. The perturbation equation is obtained by substituting Eq. (6) into Eq. (5). For the perturbation equation to have a nontrivial solution, it must be:

$$\left| \omega \mathbf{A} - k \mathbf{B} - ik^2 \mathbf{C} \right| = 0 \quad (7)$$

When the artificial viscosities are not considered ($\varepsilon_g = \varepsilon_l = \nu_g = \nu_l = 0$), Eq. (7) yields

$$\omega_l = \frac{\sqrt{\alpha_g \alpha_l \rho_g \rho_l}}{\bar{\rho}} u_R k \quad (8)$$

where ω_l is the imaginary part of the growth rate and determines the stability, $\bar{\rho} = \alpha_g \rho_l + \alpha_l \rho_g$, and $u_R = |u_g - u_l|$. The standard two-fluid model is ill-posed except for $u_R = 0$.

For non-zero artificial viscosities, the critical wavenumber can be analytically obtained as

$$k_c = \frac{\sqrt{\alpha_g \alpha_l \rho_g \rho_l (\alpha_l \varepsilon_g \nu_g \rho_g + \alpha_g \varepsilon_l \nu_l \rho_l) [\alpha_l \rho_g (\varepsilon_g + \nu_g)^2 + \alpha_g \rho_l (\varepsilon_l + \nu_l)^2]}}{(\alpha_l \varepsilon_g \nu_g \rho_g + \alpha_g \varepsilon_l \nu_l \rho_l) [\alpha_l (\varepsilon_g + \nu_g) \rho_g + \alpha_g (\varepsilon_l + \nu_l) \rho_l]} u_R \quad (9)$$

ω_l becomes negative for short waves such that $k > k_c$ and the model is well-posed. If the artificial viscosities of the two phases are assumed to be equal ($\varepsilon = \varepsilon_g = \varepsilon_l$ and $\nu = \nu_g = \nu_l$), the growth rate can also be analytically derived as

$$\omega_l = -\frac{\varepsilon + \nu}{2} k^2 + \sqrt{\frac{\alpha_g \alpha_l \rho_g \rho_l u_R^2}{\bar{\rho}^2} k^2 + \frac{(\varepsilon - \nu)^2}{4} k^4} \quad (10)$$

Then, the critical wavenumber is given by

$$k_c = \frac{1}{\sqrt{\varepsilon \nu}} \frac{\sqrt{\alpha_g \alpha_l \rho_g \rho_l}}{\bar{\rho}} u_R \quad (11)$$

Fullmer et al. [14] considered a case in which all artificial viscosities were the same ($\nu = \nu_g = \nu_l = \varepsilon_g = \varepsilon_l$) and obtained

$$\omega_{l, \text{Fullmer}} = -\nu k^2 + \frac{\sqrt{\alpha_g \alpha_l \rho_g \rho_l}}{\bar{\rho}} u_R k \quad (12)$$

$$k_{c, \text{Fullmer}} = \frac{1}{\nu} \frac{\sqrt{\alpha_g \alpha_l \rho_g \rho_l}}{\bar{\rho}} u_R \quad (13)$$

In this study, the Fullmer's method [14] is designated as "previous model."

If $\varepsilon_g = \varepsilon_l = 0$ and $\nu = \nu_g = \nu_l$ are assumed, then Eq. (10) is reduced to

$$\omega_l = -\frac{\nu}{2} k^2 + \sqrt{\frac{\alpha_g \alpha_l \rho_g \rho_l u_R^2}{\bar{\rho}^2} k^2 + \frac{\nu^2}{4} k^4} \quad (14)$$

Conversely, if $\varepsilon = \varepsilon_g = \varepsilon_l$ and $\nu_g = \nu_l = 0$ are assumed,

$$\omega_l = -\frac{\varepsilon}{2} k^2 + \sqrt{\frac{\alpha_g \alpha_l \rho_g \rho_l u_R^2}{\bar{\rho}^2} k^2 + \frac{\varepsilon^2}{4} k^4} \quad (15)$$

In Eqs. (14) and (15), as k increases, ω_l approaches zero but does not become negative. In other words, unless the artificial viscosities are applied to both the mass and momentum equations, the incompressible two-fluid model remains ill-posed.

Mathematically, even small values of the artificial viscosities render the two-fluid model well-posed. While the effect of numerical viscosity is dependent on the grid size, the artificial viscosities explicitly filter out the short waves, and the effect is independent of the grid size.

However, this method is problematic. Equations (1) and (2) are the phase-fraction equations for incompressible flow. Equations (1) and (2) can be rewritten as:

$$\frac{\partial}{\partial t} (\alpha_g \rho_g) + \frac{\partial}{\partial x} (\alpha_g \rho_g u_g) = \varepsilon_g \rho_g \frac{\partial^2 \alpha_g}{\partial x^2} \quad (16)$$

$$\frac{\partial}{\partial t} (\alpha_l \rho_l) + \frac{\partial}{\partial x} (\alpha_l \rho_l u_l) = \varepsilon_l \rho_l \frac{\partial^2 \alpha_l}{\partial x^2} \quad (17)$$

The sum of the right-hand sides of the above two equations is not zero. Even though a slight non-conservation of each phase mass is permitted because of the presence of ε_k , the total mass must be conserved to the possible maximum extent. The conservation of the total mass is crucial for the analysis of the closed reactor system. If

ϵ_g and ϵ_l are set to small values, the total mass error can be reduced. However, as shown in Eq. (9), the critical wavenumber becomes so large that the remedy for ill-posedness may not be effective.

2.2. Present artificial viscosity model

To avoid the severe problem caused by the non-conservation of the total mass, we used the mass equations as follows:

$$\frac{\partial}{\partial t}(\alpha_g \rho_g) + \frac{\partial}{\partial x}(\alpha_g \rho_g u_g) = \epsilon' \frac{\partial^2 \alpha_g}{\partial x^2} \quad (18)$$

$$\frac{\partial}{\partial t}(\alpha_l \rho_l) + \frac{\partial}{\partial x}(\alpha_l \rho_l u_l) = \epsilon' \frac{\partial^2 \alpha_l}{\partial x^2} \quad (19)$$

The sum of the right-hand sides of the above two equations is zero. The two-fluid model given by Eqs. (18), (19), (3) and (4) can be provided in the matrix form given by Eq. (5) with

$$\mathbf{A} = \begin{pmatrix} 1 & 0 & 0 & 0 \\ -1 & 0 & 0 & 0 \\ 0 & 1 & 0 & 0 \\ 0 & 0 & 1 & 0 \end{pmatrix} \quad (20)$$

$$\mathbf{B} = \begin{pmatrix} u_g & \alpha_g & 0 & 0 \\ -u_l & 0 & 1 - \alpha_g & 0 \\ 0 & u_g & 0 & 1/\rho_g \\ 0 & 0 & u_l & 1/\rho_l \end{pmatrix} \quad (21)$$

$$\mathbf{C} = \begin{pmatrix} -\epsilon'/\rho_g & 0 & 0 & 0 \\ +\epsilon'/\rho_l & 0 & 0 & 0 \\ 0 & -\nu_g & 0 & 0 \\ 0 & 0 & -\nu_l & 0 \end{pmatrix} \quad (22)$$

If $\nu = \nu_g = \nu_l$ is assumed, the critical wavenumber can be analytically obtained using Eq. (7) as follows:

$$k_c = \frac{\sqrt{\alpha_g \alpha_l [\alpha_g \rho_g (\epsilon' + \rho_l \nu)^2 + \alpha_l \rho_l (\epsilon' + \rho_g \nu)^2]}}{\sqrt{\epsilon' \nu (\epsilon' + \bar{\rho} \nu)}} u_R \quad (23)$$

ω_l becomes negative for the short waves such that $k > k_c$, and the two-fluid model is well-posed.

If $\epsilon' = \bar{\rho} \nu$ is further assumed, the growth rate can also be analytically derived as

$$\omega_l = -\nu k^2 + \frac{\sqrt{2\alpha_g \alpha_l \sqrt{\rho_g^2 \rho_l^2 u_R^4 + \nu^2 \rho^2 (\rho_l - \rho_g)^2 k^2 u_R^2} + 2\alpha_g \alpha_l \rho_g \rho_l u_R^2}}{2\bar{\rho}} k \quad (24)$$

Then, the critical wavenumber is given by

$$k_c = \frac{\sqrt{\alpha_g \alpha_l [\alpha_g \rho_g (\rho_l + \bar{\rho})^2 + \alpha_l \rho_l (\rho_g + \bar{\rho})^2]}}{2\nu \bar{\rho} \sqrt{\bar{\rho}}} u_R \quad (25)$$

However, this method may not be appropriate despite the mathematically concise expression for the growth rate. When the void fraction is so large that $\bar{\rho} = \alpha_g \rho_l + \alpha_l \rho_g$ is close to the liquid density, the large value of $\epsilon' = \bar{\rho} \nu$ may result in considerable phasic mass errors.

Hence, instead of using $\epsilon' = \bar{\rho} \nu$, we propose to assume $\epsilon' = \rho_g \nu$; the use of gas density diminishes the amount of the unwanted

phase change. Then, Eq. (23) is rewritten as

$$k_{c,Present} = \frac{\sqrt{\alpha_g \alpha_l [\alpha_g \rho_g (\rho_l + \rho_g)^2 + \alpha_l \rho_l (\rho_g + \rho_g)^2]}}{\nu \sqrt{\rho_g (\rho_g + \bar{\rho})}} u_R \quad (26)$$

In this study, the two-fluid model using $\nu = \nu_g = \nu_l$ and $\epsilon' = \rho_g \nu$ is designated as “present model.” The obvious advantages of this method are the conservation of the total mass and reduced phasic mass errors. We now compare the critical wavenumber given by Eq. (26) with that given by Eq. (13). Through algebraic manipulation, we can prove that $k_{c,Present} / k_{c,Fullmer}$ is always greater than unity. The stabilizing effect of the present model is lower than that of the previous model.

3. Results and discussion

The SPACE code is the latest thermal-hydraulics code developed by Korean nuclear industries and research institutes [15], which deals with the two-fluid and three-field governing equations that comprise gas, continuous liquid, and droplet fields. In this study, the artificial viscosities were added to the mass and momentum equations for the gas and continuous liquid fields. To eliminate the droplet effect, the rates of droplet entrainment and deposition were intentionally set to zero. Code calculations were performed for two problems to test the effects of the artificial viscosities. The virtual mass, interfacial drag, and wall drag were not considered in the code calculations.

3.1. Water-faucet flow

The water faucet problem [16] has been widely used as a benchmark to test two-fluid models or numerical methods. This problem describes the free fall of a column of water with a non-zero initial velocity in a vertical pipe. At the top inlet, the water fraction and velocity are maintained at their initial values. The water column that passes through the top inlet gradually thins as the water column velocity increases, whereas the diameter of the water column initially present in the pipe remains unchanged. There is a discontinuity in the water fraction until the water column initially present in the pipe completely exits the vertical pipe.

This study considered an air-water flow in a vertical pipe with diameter $D = 1$ m and length $L = 6$ m at atmospheric pressure and room temperature. Initially, the water fraction and velocity were assumed to be uniform as $\alpha_{l,0} = 0.8$ and $u_{l,0} = 10$ m/s, respectively. Theoretically, the distance x_d from the top inlet to the water fraction discontinuity location is given by

$$x_d = u_{l,0} t + 0.5gt^2 \quad (27)$$

The local water velocity and fraction are respectively given by

$$u_l(x, t) = \begin{cases} \sqrt{u_{l,0}^2 + 2gx}, & x < x_d \\ u_{l,0} + gt, & x \geq x_d \end{cases} \quad (28)$$

$$\alpha_l(x, t) = \begin{cases} \alpha_{l,0} u_{l,0} / u_l, & x < x_d \\ \alpha_{l,0}, & x \geq x_d \end{cases} \quad (29)$$

Unless stated otherwise, the water fraction distributions were compared at the same instant of time ($t = 0.3$ s) for different grid sizes. The test grid sizes were $\Delta x = 120$ mm (50 cells), 60 mm (100 cells), 30 mm (200 cells), 15 mm (400 cells), 7.5 mm (800 cells), 6 mm (1000 cells), and 3.75 mm (1600 cells). For each code calculation, the time step (Δt) was fixed by setting the Courant

number to u_l (0.6 m, 0.3 s) $\Delta t / \Delta x = 0.043$.

Fig. 1 compares the water fraction distributions at the same instant of time (0.3 s except for $\Delta x = 6$ mm) for different levels of grid refinement when the artificial viscosities are not considered. The steepness of the curve near the discontinuity location increases with a decrease in the grid size. However, for $\Delta x = 6$ mm, the code calculation was abnormally terminated at 0.291574 s, mainly due to the ill-posed nature and the appearance of shorter waves beyond the grid-dependent numerical viscosity. In Fig. 1, the curve of $\Delta x = 6$ mm corresponds to the data at 0.291574 s. The total mass error ratio was defined as

$$e(t) = \frac{|m_{tot} - (m_{tot,0} + m_{in} - m_{out})|}{m_{tot,0} + m_{in} - m_{out}} \times 100 \quad (30)$$

where $m_{tot,0}$, m_{tot} , m_{in} , and m_{out} denote the initial total mass in the pipe, total mass in the pipe, total mass injected from the top inlet, and total mass discharged through the bottom outlet, respectively. As shown in Fig. 1, the total mass error ratio increases abnormally immediately before the code calculation is terminated abnormally.

Fullmer et al. [14] adopted Eqs. (1)–(4) and assumed the all kinematic viscosities are the same, i.e., $\nu = \nu_g = \nu_l = \varepsilon_g = \varepsilon_l$. Further, they suggested the value of ν as

$$\nu = \frac{l}{2\pi} \frac{\sqrt{\alpha_g \alpha_l \rho_g \rho_l}}{\bar{\rho}} u_R \quad (31)$$

Although the filter length l depends on the flow, the choice $l = 2D$ is generally acceptable as an upper bound on the filter length. We adopted $l = 2D$. Fig. 2 shows the results when the previous model is used. Because of the presence of artificial viscosities ($\nu \sim 0.2 \text{ m}^2/\text{s}$), the water fraction distributions are smoother, and the code calculation with $\Delta x = 3.75$ mm successfully continues until 0.3 s. However, because the coefficient on the right-hand side of Eq. (17) is as large as $\varepsilon_l \rho_l = \nu \rho_l \sim 200 \text{ kg/m}\cdot\text{s}$, the total mass error ratio increases to 0.03%. In view of the short calculation time (0.3 s), this level of mass error may cause a serious problem in the long-

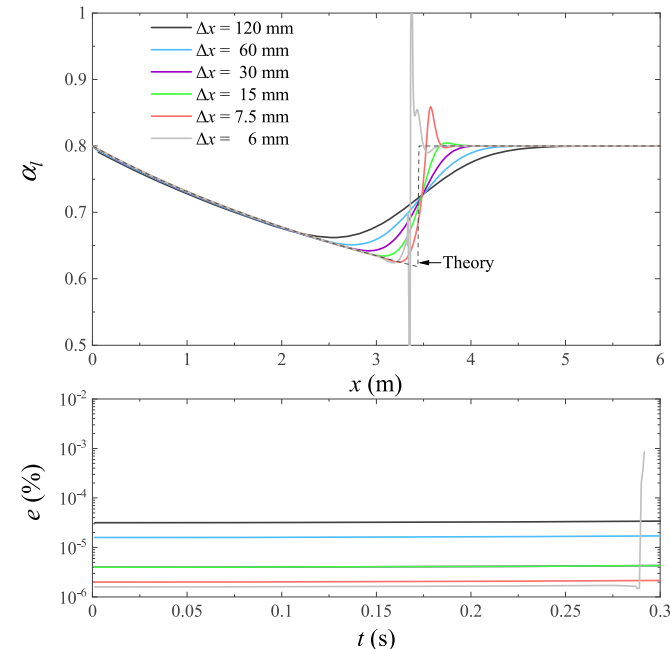


Fig. 1. Water fraction and total mass error ratio when artificial viscosities are not considered.

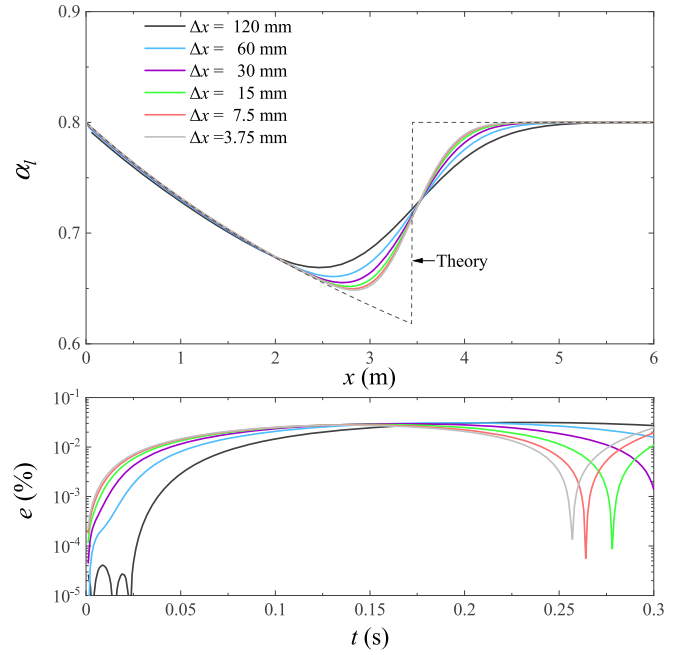


Fig. 2. Water fraction and total mass error ratio when the previous model is used.

term simulations of the closed reactor system. Therefore, the mass error problem must be resolved.

Fig. 3 shows the results when the proposed model is used. The value of ν is determined using Eq. (31) and $l = 2D$. As discussed in Section 2.2, the advantages of the present method are the conservation of total mass and reduction in phasic mass errors. As shown in Fig. 3, the water fraction is well predicted even with $\Delta x = 3.75$ mm (1600 cells). Compared with the water fraction distributions shown in Fig. 2, the water fraction curves are closer to the theoretical line. As the grid is refined, the results converge. In particular, the total mass error ratios reduce significantly because

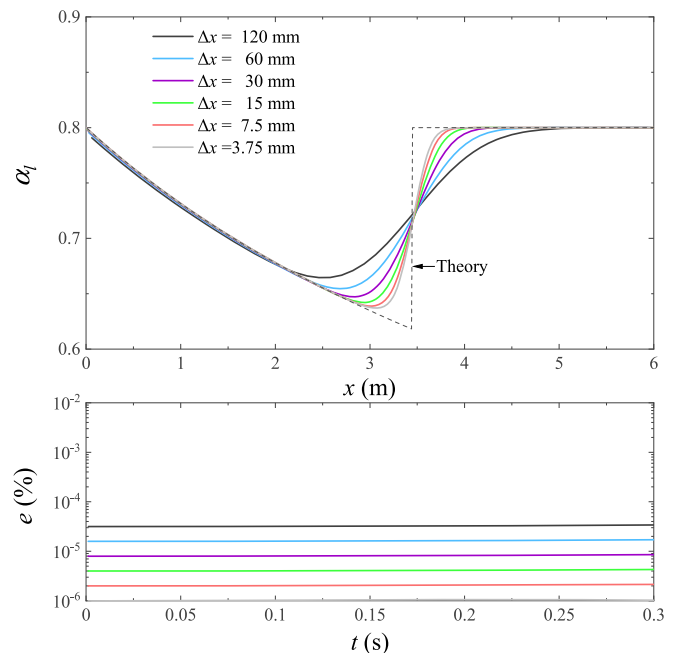


Fig. 3. Water fraction and total mass error ratio when the present model is used.

the coefficient on the right-hand side of Eq. (19) is as small as $e' = \rho_g \nu \sim 0.2 \text{ kg/m}\cdot\text{s}$. Fig. 3 clearly demonstrates the advantages of the present model.

3.2. Kelvin-Helmholtz instability

An unstable flow in a horizontally stratified channel, known as Kelvin-Helmholtz instability, was considered. To simulate this flow, $\alpha_g \rho_g g_y H \partial \alpha_g / \partial x$ and $-\alpha_l \rho_l g_y H \partial \alpha_l / \partial x$ were added to the right-hand sides of Eqs. (3) and (4), respectively, to account for the hydrostatic pressure effect, where H is the cross-sectional channel size. Because the theory is well known, a detailed dispersion analysis is not described here.

This study considered an air–water flow in a rectangular horizontal channel at atmospheric pressure and room temperature. The channel height and length were $H = 2.5 \text{ cm}$ and $L = 0.5 \text{ m}$, respectively. Two sides of the pipe were connected to each other. Initially, the water fraction was set as follows:

$$\alpha_l = \begin{cases} 0.5 + 0.01 \sin[2\pi(x - 0.1)/0.1] & , 0.1 \leq x < 0.2 \text{ m} \\ 0.5 & , \text{ otherwise} \end{cases} \quad (32)$$

A long wave with a small amplitude was present in the stratified interface. For the inviscid and incompressible flow, the critical relative velocity for stability is calculated as

$$|u_g - u_l|_{crit} = \sqrt{\frac{\bar{\rho}(\rho_g - \rho_l)gH}{\rho_g \rho_l}} = 10.3 \text{ m/s} \quad (33)$$

If the relative velocity is larger than the critical velocity, the flow becomes unstable and the wave grows over time. The initial air and water velocities were set to 13.0 m/s and 1.0 m/s, respectively, to consider an unstable flow. Interestingly, the critical condition is identical to the onset condition of the ill-posedness of the two-fluid model without artificial velocities. The test grid sizes were $\Delta x = 10 \text{ mm}$ (50 cells), 4 mm (125 cells), 2 mm (250 cells), 1 mm (500 cells), 0.5 mm (1000 cells), and 0.25 mm (2000 cells). For each code calculation, the time step (Δt) was fixed by setting the Courant number to 0.26.

Fig. 4 shows the spatial and temporal evolution of the long wave when the artificial viscosities are not considered. The time interval between the curves is 0.02 s. For $\Delta x = 10 \text{ mm}$, the wave decays marginally in the early stage and propagates while maintaining the amplitude. Supposedly, the flow instability and grid-dependent numerical viscosity are balanced. The smaller the grid size, the more rapidly the wave grows. For $\Delta x = 1 \text{ mm}$, 0.5 mm, and 0.25 mm, the code calculations were abnormally terminated at 0.161076, 0.0999954, and 0.0570595 s, respectively, which may be due to the dominant effect of the ill-posed nature against the numerical viscosity effect. It is shown in Fig. 5 that the mass error ratio increases abruptly immediately before the code calculation is terminated abnormally.

Figs. 6 and 7 show the results of the previous model based on Eqs. (1), (2), (3), and (4). All calculations are successfully continued until 0.2 s. For $\Delta x = 10 \text{ mm}$, the wave tends to decay continuously. For other grid sizes, the waves decay marginally in the early stage and propagate while maintaining their amplitudes. The large stabilizing effect of the previous model might be acceptable in view of the code calculation success. However, the total mass error ratio, as shown in Fig. 7, reaches 0.01%. This level of mass error may cause serious problems in the long-term simulations of the closed reactor system.

Now, we turn to the present model. The results of the present model based on Eqs. (18), (19), (3), and (4) are shown in Figs. 8 and

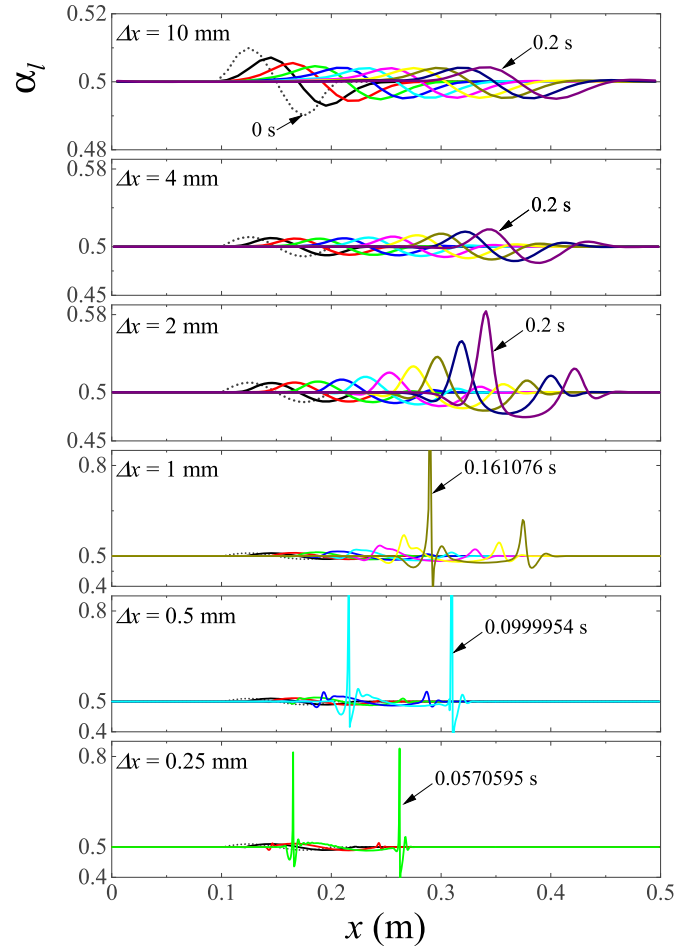


Fig. 4. Evolution of the water wave when artificial viscosities are not considered.

9, respectively. The wave growth over time is successfully predicted, except for $\Delta x = 10 \text{ mm}$. The artificial viscosities of the present model enable the simulation of the unstable wave. The mass errors are negligible, as shown in Fig. 9. The present model has less stabilizing effect than the previous model but renders the two-fluid model well-posed. More importantly, the total mass error

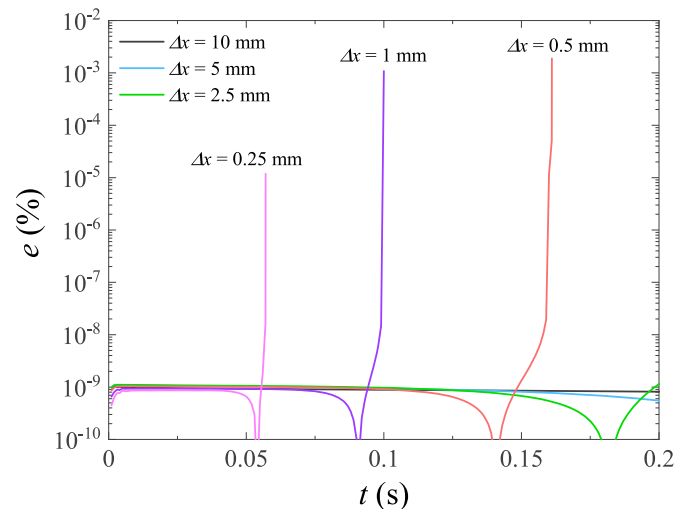


Fig. 5. Mass error ratio over time when the artificial viscosities are not considered.

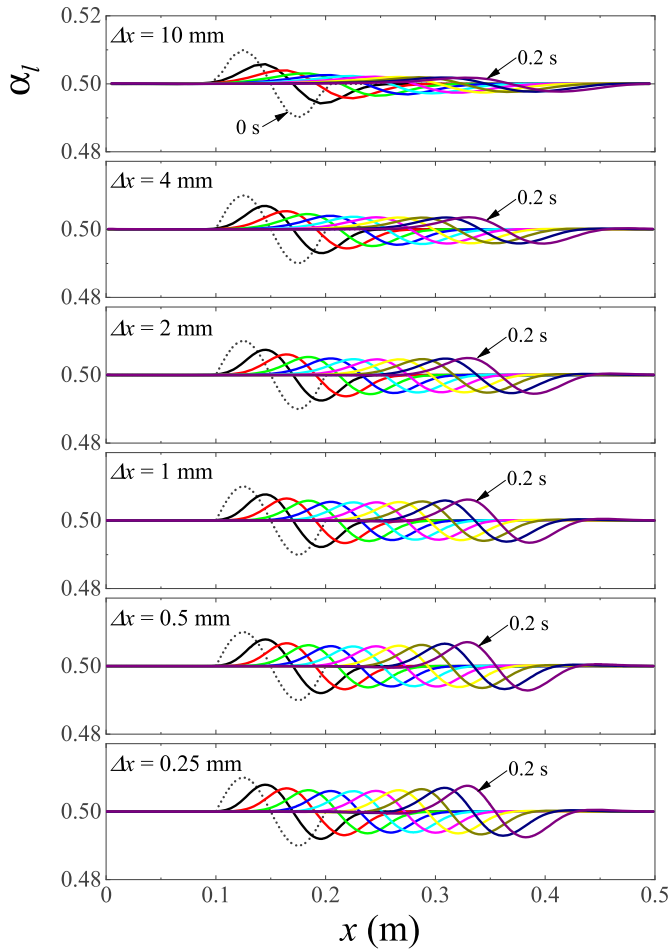


Fig. 6. Evolution of the water wave when the previous model is used.

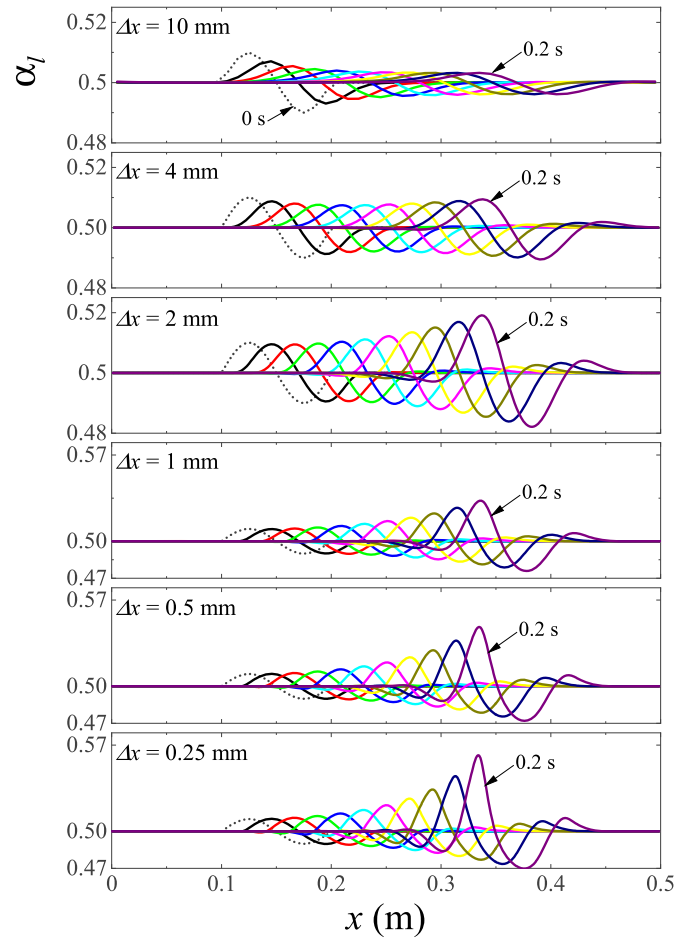


Fig. 8. Evolution of the water wave when the present model is used.

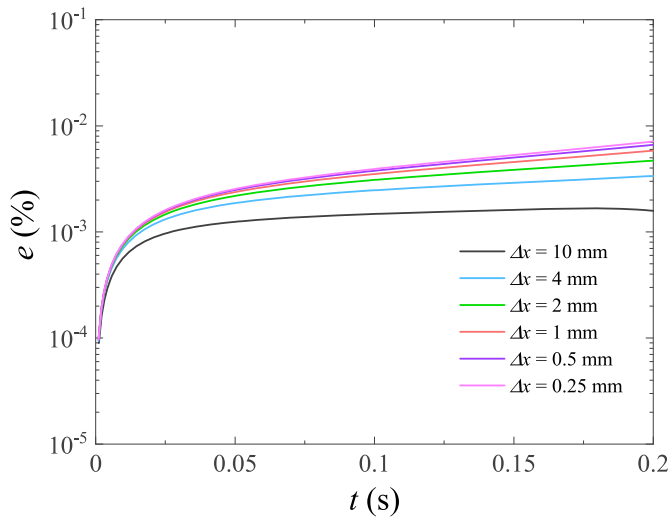


Fig. 7. Mass error ratio over time when the previous model is used.

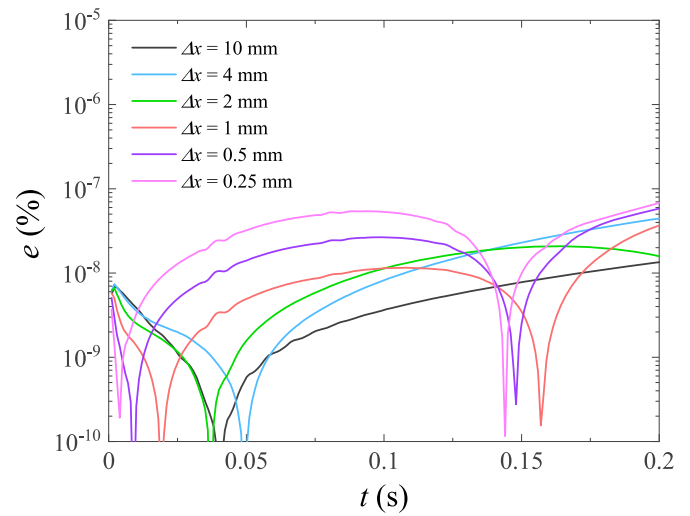


Fig. 9. Mass error ratio over time when the present model is used.

is significantly reduced.

Fig. 10 compares the water fraction distributions along the channel at the same instant of time (0.1 s) for different levels of grid refinement of different two-fluid models. For the model without artificial viscosities, as shown in Fig. 10 (a), the curves do not converge, and large fluctuations of α_l are observed in the curve of

$\Delta x = 0.5$ mm. However, for the present model shown in Fig. 10 (c), the curves are smooth and converge as the grid is refined, demonstrating that the proposed well-posed model is appropriate.

So far, we have showed that the present two-fluid model remedies the ill-posedness and mass conservation error. Vaidheeswaran and de Bertodano [17] developed a well-posed two-fluid model for flow bubbly flows based on bubble collision

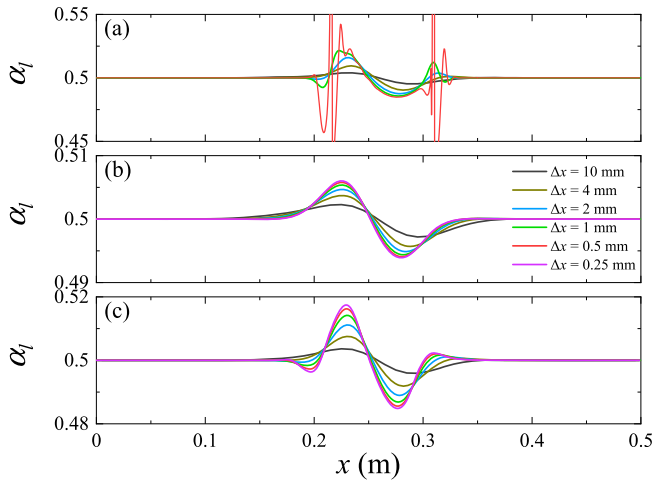


Fig. 10. Water fraction along a channel at the same instant of time (0.1 s) for different levels of grid refinement: (a) no artificial viscosities are considered, (b) previous model, (c) present model.

mechanism. The analysis with one-dimensional two-fluid model was extended to a multi-dimensional CFD application, and the grid convergence was shown to be feasible. Considering the previous work, it is expected that the present one-dimensional two-fluid model concept can be extended to a multi-dimensional CFD applications.

4. Conclusions

The artificial viscosities in both the mass and momentum equations render the two-fluid model well-posed. However, the total mass was not conserved in the previous artificial viscosity model. Non-conservation of the total mass may cause serious problems in the analysis of the closed reactor system.

To resolve this problem, we suggested using the following mass equations (Eqs. (18) and (19)):

$$\frac{\partial}{\partial t}(\alpha_g \rho_g) + \frac{\partial}{\partial x}(\alpha_g \rho_g u_g) = \epsilon' \frac{\partial^2 \alpha_g}{\partial x^2}$$

$$\frac{\partial}{\partial t}(\alpha_l \rho_l) + \frac{\partial}{\partial x}(\alpha_l \rho_l u_l) = \epsilon' \frac{\partial^2 \alpha_l}{\partial x^2}$$

For $\epsilon' = \rho_g \nu$, the critical wavenumber based on linear stability analysis was obtained (Eq. (26)) as follows:

$$k_c = \frac{\sqrt{\alpha_g \alpha_l [\alpha_g \rho_g (\rho_l + \rho_g)^2 + \alpha_l \rho_l (\rho_g + \rho_g)^2]}}{\nu \sqrt{\rho_g (\rho_g + \bar{\rho})}} u_R$$

Compared with the previous artificial viscosity model, the present artificial viscosity model reduced both total and phasic mass errors.

The water faucet problem was simulated to verify the effects of the present model. Compared with the water fraction distributions of the previous model, those of the present model were closer to the theoretical line. Moreover, the total mass error was significantly reduced.

An unstable flow in a horizontally stratified channel was simulated. In the previous model, the waves decayed marginally in the early stage and propagated while maintaining their amplitudes. The large stabilizing effect of the previous model might be acceptable considering the code calculation success. However, the

total mass error ratio reached 0.01%. This level of mass error may cause serious problems in the long-term simulations of the closed reactor system. However, the present artificial viscosity model successfully demonstrated the growth of unstable waves. More importantly, the mass errors were negligible. In particular, the water fraction distributions at the same instant of time were smooth and nearly converged as the grid was refined.

From the results, we conclude that the proposed artificial viscosity model effectively remedies the ill-posedness of the two-fluid model while maintaining a negligible total mass error.

Declaration of competing interest

The authors declare that they have no known competing financial interests or personal relationships that could have appeared to influence the work reported in this paper.

Acknowledgments

This work was supported by the National Research Foundation of Korea grants funded by the Ministry of Science and ICT (No. NRF-2021M2D2A1A02039565). This work was supported by the Korea Institute of Energy Technology Evaluation and Planning (KETEP) grant funded by the Korea government (MOTIE) (20214000000090, Fostering human resources training in advanced hydrogen energy industry).

References

- [1] R.W. Lyczkowski, D. Gidaspo, C.W. Solbrig, E.D. Hughes, Characteristics and stability analyses of transient one-dimensional two-phase flow equations and their finite difference approximations, *Nucl. Sci. Eng.* 66 (1978) 378–396.
- [2] J.D. Ramshaw, J.A. Trapp, Characteristics, stability, and short-wavelength phenomena in two-phase flow equation systems, *Nucl. Sci. Eng.* 66 (1978) 93–102.
- [3] T. Watanabe, Y. Kukita, The effect of the virtual mass term on the stability of the two-fluid model against perturbations, *Nucl. Eng. Design* 135 (1992) 327–340.
- [4] D. Barnea, Y. Taitel, Kelvin-helmholtz stability criteria for stratified flow: viscous versus non-viscous (inviscid) approaches, *Int. J. Multiphase Flow* 19 (1993) 639–649.
- [5] S.Y. Kadioglu, R. Nourgaliev, N. Dinh, A Novel Hyperbolization Procedure for the Two-phase Six-Equation Flow Model, 2011. INL/EXT-11-23551; TRN: US1200674.
- [6] S.-J. Lee, K.-S. Chang, S.-J. Kim, Surface tension effect in the two-fluids equation system, *Int. J. Heat Mass Tran.* 41 (1998) 2821–2826.
- [7] V.H. Ransom, D.L. Hicks, Hyperbolic two-pressure models for two-phase flow, *J. Comput. Phys.* 53 (1984) 124–151.
- [8] R.A. Berry, L. Zou, H. Zhao, H. Zhang, J.W. Peterson, R.C. Martineau, S.Y. Kadioglu, D. Andrs, Relap-7 Theory Manual, 2016. INL/EXT-14-31366 (Revision 2).
- [9] J.H. Song, A remedy for the ill-posedness of the one-dimensional two-fluid model, *Nucl. Eng. Design* 222 (2003) 40–53.
- [10] J. Michael Doster, M.A. Holmes, Numerical stability of the six-equation, single-pressure model with viscous terms, *Nucl. Sci. Eng.* 124 (1996) 125–144.
- [11] USNRC, Relap5/Mod3.3 Code Manual Vol. I: Code Structure, System Models, and Solution Methods, Nuclear Regulatory Commission, 2016. NUREG/CR-5535/Rev P5-Vol I.
- [12] H. Holmås, T. Sira, M. Nordsveen, H.P. Langtangen, R. Schulkes, Analysis of a 1d incompressible two-fluid model including artificial diffusion, *IMA J. Appl. Mathemat. (Inst. Mathemat. Applicat.)* 73 (2008) 651–667.
- [13] W.D. Fullmer, V.H. Ransom, M.A. Lopez de Bertodano, Linear and nonlinear analysis of an unstable, but well-posed, one-dimensional two-fluid model for two-phase flow based on the inviscid kelvin–helmholtz instability, *Nucl. Eng. Design* 268 (2014) 173–184.
- [14] W.D. Fullmer, S.Y. Lee, M.A.L.D. Bertodano, An artificial viscosity for the ill-posed one-dimensional incompressible two-fluid model, *Nucl. Technol.* 185 (2014) 296–308.
- [15] S.J. Ha, C.E. Park, K.D. Kim, C.H. Ban, Development of the space code for nuclear power plants, *Nucl. Eng. Technol.* 43 (2011) 45–62.
- [16] V.H. Ransom, Numerical benchmark test No. 2.1, Faucet Flow 3 (1987) 465–467.
- [17] A. Vaidheeswaran, M.L. de Bertodano, Stability and convergence of computational eulerian two-fluid model for a bubble plume, *Chem. Eng. Sci.* 160 (2017) 210–226.